Solar Polarization 7
ASP Conference Series, Vol. 489
K. N. Nagendra, J. O. Stenflo, Zhongquan Qu, and M. Sampoorna, eds.

Fast Solar Polarimeter: Description and First Results

A. Feller,[1] F. A. Iglesias,[1] K. Nagaraju,[1] S. K. Solanki,[1,2] and S. Ihle[3]

[1]*Max-Planck-Institut für Sonnensystemforschung, Justus-von-Liebig-Weg 3, 37077 Göttingen, Germany*
[2]*School of Space Research, Kyung Hee University, Yongin, 446-701 Gyeonggi, Republic of Korea*
[3]*PNSensor GmbH, 80803 Munich, Germany*

Abstract. We are developing a novel fast solar imaging polarimeter with an emphasis on significantly increased polarimetric accuracy and high spatial resolution. The instrument is based on a fast pnCCD sensor and shall work at frame rates of up to 400 fps, which suppresses spurious polarization signals induced by external disturbances such as atmospheric turbulence or jitter. The much higher polarimetric accuracy that can be achieved with the new instrument is in particular expected to extend studies of the enigmatic small-scale magnetic field in the quiet Sun, and of chromospheric magnetic fields. Here we will report on some key concepts of the polarimeter, and on first results obtained with an evaluation model at the spectrograph of the Vacuum Tower Telescope on Tenerife.

1. Introduction

Polarization measurements from the ground are well known to suffer from image instabilities due to atmospheric seeing and jitter, which can seriously affect polarimetric accuracy (cf. Lites 1987; Judge et al. 2004; Casini et al. 2012) and spatial resolution. As shown by Nagaraju & Feller (2012), adaptive optics correction with a limited number of modes does not alleviate the requirements on the modulation frequency of a polarimeter. If the effective exposure time of individual frames is smaller than the seeing time scale (∼10 ms) and if simultaneous 2D spatial information is available (e.g., using filtergraph type instruments), residual spatial smearing can be mitigated with post-facto image reconstruction techniques such as speckle interferometry (e.g., Keller & von der Luehe 1992; von der Luehe 1993; Wöger et al. 2008), phase diversity (e.g. Gonsalves & Chidlaw 1979; Löfdahl & Scharmer 1994), or Multi-Object Multi-Frame Blind Deconvolution (MOMFBD; van Noort et al. 2005).

Different techniques have been implemented to suppress spurious polarization signals. Dual-beam polarimeters allow to efficiently reduce crosstalk from Stokes I to Stokes Q, U, V and, when combined with beam-exchange techniques (e.g., Semel et al. 1993), differential gain table and imaging effects between the two beams can be suppressed as well. However in case of slow temporal modulation, beam exchange may result in spatial smearing when the images to be combined span a period larger than the typical seeing time scale. The Zurich Imaging Polarimeter (ZIMPOL; cf. Povel et al. 1994; Gandorfer & Povel 1997; Ramelli et al. 2010) relies on very fast single-beam

Table 1. Verified and expected specifications of the present pnCCD evaluation model (Phase I) and of the future large scale sensor (Phase II), respectively.

	Phase I	Phase II
Sensor size (pixels)	264×264	1024×1024
Pixel size (μm)	48	36
Maximum frame rate (fps)	850	400
Quantum efficiency > 0.9	550 - 800 nm	380 - 650 nm (goal)
Readout noise	~ 3 e$^-$ rms	
Residual non-linearity, after calibration	$< 10^{-2}$	
Duty cycle	0.95	0.9

modulation. At modulation frequencies up to 40 kHz, which can be reached with the ZIMPOL charge-shifting technique, any seeing induced effects on polarimetric accuracy become completely negligible. Using long integration combined with substantial spatial averaging, it is possible to reduce the noise level of ZIMPOL data to the order of 10^{-5}, which allows for an in-depth analysis of the faint scattering polarization signatures of the Second Solar Spectrum. However, due to its low cadence and its small duty cycle at short exposures, the current version of ZIMPOL is not ideally suited for observations close to the diffraction limit, relying on image reconstruction. Other shortcomings in the context of high-resolution imaging are the reduced number of effective pixels and their highly asymmetric shape.

2. Development of a Novel Fast Solar Polarimeter

In collaboration with the semiconductor lab (HLL) of the Max Planck Society and with PNSensor corp., we are developing a novel imaging polarimeter for ground-based solar observations. The key component of the instrument is a fast and low-noise pnCCD camera (e.g., Hartmann et al. 2006; Ihle et al. 2012), which can be operated at modulation frequencies in the 100 Hz range (cf. Table 1). The polarization modulator is based on 2 ferro-electric liquid crystals, closely following the SOLIS design (Keller et al. 2003; Gisler 2005), and allows for a quasi-simultaneous and efficient measurement of the full Stokes vector at the above frame rates. The Fast Solar Polarimeter (FSP) mainly aims for high-precision polarimetry down to an accuracy level of about $1 \cdot 10^{-4}$ in polarization degree, combined with high spatial resolution. In this sense FSP is complementary to other solar polarimeters.

The FSP development is split into two phases, of which phase I is ongoing. An evaluation model has already been implemented, based on a pnCCD with reduced sensor dimensions of 264 x 264 pixels. This instrument allows us to assess the actual performance of the new measurement concept in a single-beam configuration, and to gain practical experiences which will be valuable for the next project phase. Phase II aims at the development of a full-scale science ready instrument, based on two 1k x1k pnCCDs in a dual-beam configuration.

Table 2. FSP photon budget for 3 selected spectral regions. In all examples we assume Nyquist sampling of the diffraction limited point spread function, 10% overall throughput (including the sensor quantum efficiency), an exposure time of 2.5 ms per frame (400 fps), a spectral equivalent width of 100 mÅ, and a polarimetric efficiency of 0.5. Further we consider the expected flux at line center, based on the line depths of the FTS atlas by Kurucz et al. (1984), and on solar irradiance data (Neckel & Labs 1984).

Example	Ca II K 393.3 nm	Fe I 525.02 nm	Ca II 854.2 nm
Intensity (photons $\cdot$ s $\cdot$ m^{-2} $\cdot$ nm^{-1} $\cdot$ sterad)	$7.9 \cdot 10^{20}$	$1.9 \cdot 10^{22}$	$1.3 \cdot 10^{22}$
Flux ($e^- \cdot$ pixel$^{-1} \cdot$ frame^{-1})	90	3800	6700
Number of pixels to average for 10^{-4} polarization sensitivity, after 1s integration	$1.1 \cdot 10^4$	260	150

The main specifications of the pnCCD are summarized in Table 1. The high frame rates are enabled by a split frame transfer mode, and by the parallel readout of all sensor columns (cf. Hartmann et al. 2006). The excellent noise characteristics allow for photon-noise limited observations at maximum frame rate, even in strong chromospheric lines, as shown by the photon budget in Table 2. The strict requirement on residual non-linearity is needed to avoid sensor induced polarization crosstalk (Keller 1996). The very high duty cycle guarantees an efficient use of the available photons within a given integration time, which is of particular importance for observations of faint magnetic fields in the highly dynamic chromosphere. In case of quasi-monochromatic observations, the thick sensor substrate eliminates the risk of fringing in the back-illuminated sensor.

The measured modulation efficiencies (cf. del Toro Iniesta & Collados 2000) of Stokes Q, U, and V have average values of about 0.53, 0.49, and 0.5 respectively, and are subject to some 2-4% relative changes with modulation frequency, and to some 10-20% relative changes with wavelength (within the measured range 400 nm - 650 nm).

3. Scientific Focus

As shown in Table 2, the limited photon flux makes it impossible to reach a polarimetric accuracy of order 10^{-4} on a per-pixel base within the intrinsic sub-arcsec solar evolution time scale, without compromising spectral or spatial resolution. To reach such an increased polarimetric accuracy level, combined with small-scale spatial information, we will therefore explore, in future work with FSP, the potential of statistical approaches. The basic idea is to perform feature based spatial averages (e.g., granules versus intergranular lanes). As an example of a potential application we note the predicted fluctuations of scattering polarization in Sr I 460.7 nm (Trujillo Bueno & Shchukina 2007) on granular and sub-granular scales. A first observational hint of this effect, which sets

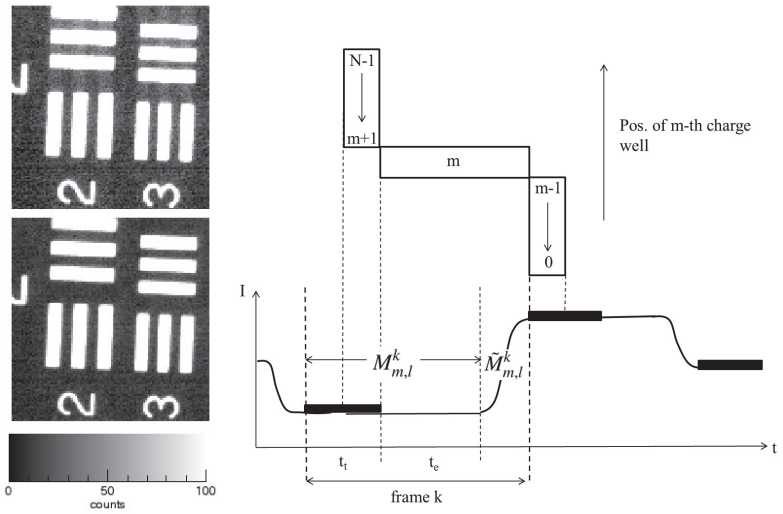

Figure 1. *Left panel*: USAF target image affected by frame transfer effects in the vertical direction (top), and corrected image (bottom). The image was recorded at 700 fps. *Right panel*: Schematic overview of the measurement process, including frame transfer and finite modulator transition. The black boxes on the intensity plot denote the frame transfer phases. All other annotations are explained in the text.

important constraints on magneto-hydrodynamical and radiative transfer modeling of the lower solar atmosphere, has been reported in the CN band by Snik et al. (2010).

Another option, which is particularly interesting for chromospheric studies, is to track the evolution of a given solar feature, and to average the corresponding pixels in space and time, trading spatial resolution against cadence as needed. Feature tracking techniques have already been employed to study small-scale magnetic structures like, e.g., chromospheric bright points (e.g., Jafarzadeh et al. 2013), or the still enigmatic magnetic fields on sub-granular scales in the quiet Sun photosphere (e.g., Anusha et al. 2014). Highly resolved individual frames, allowing a clear discrimination of small-scale structures, are a common essential requirement of all those techniques.

4. Calibration and Measurement Issues

The complications of mechanical or optical shuttering at high frame rates lead us to operate the FSP camera without a shutter. This however necessitates a post-facto frame transfer correction. After exposure, the photocharges, accumulated in the light sensitive sensor area, are shifted to the shielded storage area for readout. As the sensor pixels continue being exposed during the transfer, the image suffers from a spatial smearing along the transfer direction, as shown in Fig. 1 (streaks in vertical direction, in upper left panel). We note that the effect is different for each modulation state and implies a spatial crosstalk in the range of 1 – 2% (depending on frame rate) which cannot be eliminated in terms of the usual polarimeter calibration performed for each pixel independently.

For time-independent intensity images, correction algorithms have been developed by Powell et al. (1999) and Ruyten (1999). These algorithms are however not applica-

ble to our case of intensity modulated images, in particular in the presence of strong contrasts in the polarization signals.

Due to the specific behavior of our sensor, our calibration technique differs substantially from the techniques used for other polarimeters. In this section we sketch the basic problem, the details of the calibration algorithm, and its practical performance will be described in a later publication.

Figure 1 illustrates the measurement process. Pixel m of frame k is statically exposed during the time t_e, and then transferred to the storage area. To transfer all N pixels of a given column a time t_t is needed. Pixel m thus suffers from spatial crosstalk from frame $k+1$. In a similar way spatial crosstalk within frame k is generated by the frame transfer preceding the static exposure.

An additional complication is introduced by the finite transition times of the modulator between two states. However, as the transitions are repeatable, we can describe the modulator with two independent matrices $\mathbf{M}$ and $\tilde{\mathbf{M}}$ describing the static and the transition phases respectively.

The number of photocharges I_m^k collected in pixel m of frame k can be described, to a high degree of accuracy, as:

$$\begin{aligned} I_m^k &= D_m + \sum_{l=0}^{3} g_m \left(t_e \, M_{m,l}^k + \tilde{M}_{m,l}^k \right) S_{m,l} \\ &+ \frac{tt}{N} \sum_{l=0}^{3} \left(\sum_{j=0}^{m-1} M_{j,l}^{k+1} \, g_j \, S_{j,l} + \sum_{j=m+1}^{N-1} M_{j,l}^k \, g_j \, S_{j,l} \right). \end{aligned} \tag{1}$$

The dark frame D_m, the unpolarized gain table g_m, and the two field-dependent modulator matrices $\mathbf{M}$, $\tilde{\mathbf{M}}$, can be accurately determined in practicable calibration steps at the telescope. The terms $S_{m,l}$ denote the true flux of the Stokes parameter l into pixel m, where the index $l = 0, \ldots 3$ corresponds to Stokes I, Q, U, and V respectively. With all instrumental parameters determined by calibration, and due to the strictly periodic behavior of the modulator matrices, Eq. (1) boils down to a closed linear system of equations of the form $\mathbf{I} = \mathbf{U}.\mathbf{S}$ which we can solve for the unknown Stokes vector $\mathbf{S}$.

We assume time-independent Stokes fluxes during a given modulation cycle, which is true to a sufficiently high degree of accuracy in case of fast modulation in the 100 Hz range (cf. Nagaraju & Feller 2012). We also note that we interpret the true Stokes flux as the flux entering the modulator. Any polarization crosstalk generated by preceding telescope optics, or any spatial crosstalk induced by seeing and straylight are considered in separate data reduction steps and are not described here. Ongoing developments will allow for an extension of the spatially coupled inversion technique of van Noort (2012) to ground-based observations. This new combination of the inversion problem of polarized radiative transfer with image reconstruction, will permit us to even better constrain the spatial distribution of the inferred physical parameters in the solar atmosphere.

5. First Results with the FSP Evaluation Model

Figure 2 shows an example measurement of scattering polarization in the Ca II 422.7 nm line at a $\mu = 0.15$ (+0.03, −0.05), recorded with the FSP evaluation model at the spectrograph of the Vacuum Tower Telescope (VTT) on Tenerife. The spectral sampling of these observations is about 17 mÅ per pixel. The spectra of intensity and linear

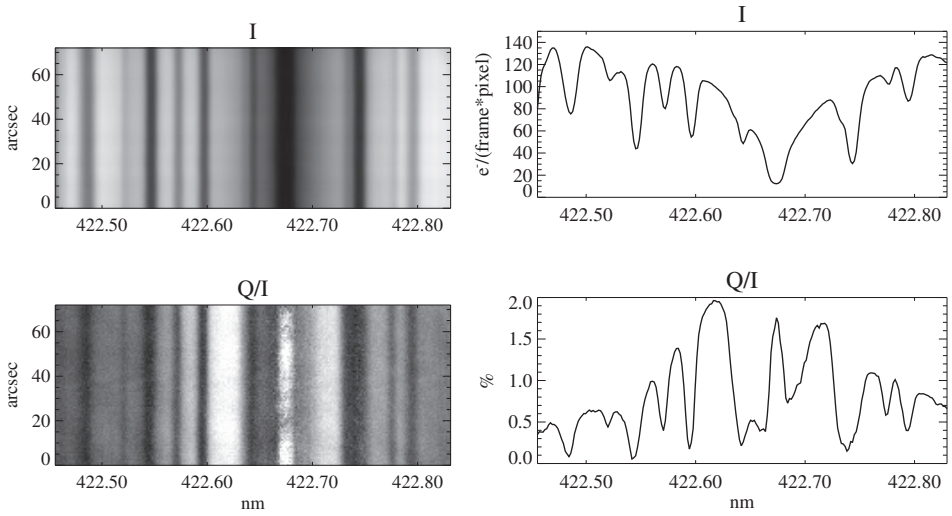

Figure 2. Second Solar Spectrum of Ca II 422.7 nm at $\mu \approx 0.15$, recorded with the FSP evaluation model during its first-light campaign at the VTT spectrograph. *Left panel*: 2D spectra in intensity and linear polarization parallel to the solar limb. *Right panel*: Spatially averaged spectra. The greyscales of the 2D spectra correspond to the plot ranges of the averaged spectra.

polarization parallel to the solar limb are the result of frame averaging, corresponding to a total effective integration time of 20 minutes. The resulting noise levels, about $7 \cdot 10^{-4}$ and $9 \cdot 10^{-5}$ in the 2D and averaged Q/I spectra respectively, are consistent with photon noise. The agreement with the ZIMPOL based atlas of the Second Solar Spectrum (Gandorfer 2002) is excellent, except for a slight scaling difference in the amplitudes, which could be due to the uncertainty in the μ value.

6. Conclusions and Outlook

The FSP evaluation model has performed reliably, without major technical issues, during its first-light campaign at the VTT spectrograph in June 2013. Shutterless operation with frame transfer correction works well, but the polarimeter calibration will still benefit from further improvements, in particular taking into account spatial variations in modulator response including polarized fringes. The polarimetric efficiencies are close to the theoretical expectations and the stable modulator response requires only few re-calibrations during an observing campaign. Test observations of a pore region at different modulation frequencies (discussed in detail in a later publication) have clearly shown that a frame rate of order 400 fps (100 Hz modulation frequency) is crucial to reach a polarimetric accuracy of order 10^{-4} in the presence of high-contrast targets, as expected from simulations (Nagaraju & Feller 2012). Based on the first-light measurements with our FSP evaluation model, we were able to demonstrate so far that a polarimetric accuracy of $1 - 2 \cdot 10^{-4}$ can be reached for spatially averaged spectra. However, at a noise level of 10^{-3} and below, we can identify instrumental artifacts, mainly related to the pnCCD camera, which need further assessment.

Our work with the FSP evaluation model will continue. First observations with the TESOS filtergraph at VTT in November 2013 shall allow us to check the real performance of the polarimeter in the regime of high-resolution imaging. Based on these observations we will be able to test different image reconstruction techniques and to assess the potential of statistical approaches to increase polarimetric accuracy while conserving some small-scale spatial information. In 2014 the phase-II hardware developments will be started, and we expect first-light observations with the full-scale instrument in early 2016.

Acknowledgments. The Fast Solar Polarimeter is funded by the Max Planck Society (MPG) and by the European Commission, grant no. 312495 (SOLARNET). We also would like to thank all the technical contributors not listed as co-authors for their invaluable input to the project.

References

Anusha, L. S., Feller, A., Hirzberger, J., & Solanki, S. K. 2014, these proceedings
Casini, R., de Wijn, A. G., & Judge, P. G. 2012, ApJ, 757, 45
del Toro Iniesta, J. C., & Collados, M. 2000, Appl.Optics, 39, 1637
Gandorfer, A. 2002, The Second Solar Spectrum: A high spectral resolution polarimetric survey of scattering polarization at the solar limb in graphical representation. Volume II: 3910 Å to 4630 Å (Zurich: vdf Hochschulverlag)
Gandorfer, A. M., & Povel, H. P. 1997, A&A, 328, 381
Gisler, D. 2005, Ph.D. thesis, ETH Zurich
Gonsalves, R. A., & Chidlaw, R. 1979, in Applications of digital image processing III, edited by A. G. Tescher (Washington D.C.: SPIE), vol. 207 of SPIE Conference Series, 32
Hartmann, R., Buttler, W., Gorke, H., Herrmann, S., Holl, P., Meidinger, N., Soltau, H., & Strüder, L. 2006, Nuclear Instruments and Methods in Physics Research Section A, 568, 118
Ihle, S., Ordavo, I., Bechteler, A., Hartmann, R., Holl, P., Liebel, A., Meidinger, N., Soltau, H., Strüder, L., & Weber, U. 2012, in High Energy, Optical, and Infrared Detectors for Astronomy V, edited by A. D. Holland, & J. W. Beletic (Washington D.C.: SPIE), vol. 8453 of SPIE Conference Series, 84531A
Jafarzadeh, S., Solanki, S. K., Feller, A., Lagg, A., Pietarila, A., Danilovic, S., Riethmüller, T. L., & Martínez Pillet, V. 2013, A&A, 549, A116
Judge, P. G., Elmore, D. F., Lites, B. W., Keller, C. U., & Rimmele, T. 2004, Appl.Optics, 43, 3817
Keller, C. U. 1996, Solar Phys., 164, 243
Keller, C. U., Harvey, J. W., & Giampapa, M. S. 2003, in Innovative Telescopes and Instrumentation for Solar Astrophysics, edited by S. L. Keil, & S. V. Avakyan (Washington D.C.: SPIE), vol. 4853 of SPIE Conference Series, 194
Keller, C. U., & von der Luehe, O. 1992, A&A, 261, 321
Kurucz, R. L., Furenlid, I., Brault, J., & Testerman, L. 1984, Solar flux atlas from 296 to 1300 nm (New Mexico: National Solar Observatory)
Lites, B. W. 1987, Appl.Optics, 26, 3838
Löfdahl, M. G., & Scharmer, G. B. 1994, A&AS, 107, 243
Nagaraju, K., & Feller, A. 2012, Appl.Optics, 51, 7953
Neckel, H., & Labs, D. 1984, Solar Phys., 90, 205
Povel, H. P., Keller, C. U., & Yadigaroglu, I.-A. 1994, Appl.Optics, 33, 4254
Powell, K., Chana, D., Fish, D., & Thompson, C. 1999, Appl.Optics, 38, 1343
Ramelli, R., Balemi, S., Bianda, M., Defilippis, I., Gamma, L., Hagenbuch, S., Rogantini, M., Steiner, P., & Stenflo, J. O. 2010, in Ground-based and Airborne Instrumentation for Astronomy III, edited by I. S. McLean, S. K. Ramsay, & H. Takami (Washington D.C.: SPIE), vol. 7735 of SPIE Conference Series, 77351Y

Ruyten, W. 1999, Optics Letters, 24, 878
Semel, M., Donati, J.-F., & Rees, D. E. 1993, A&A, 278, 231
Snik, F., de Wijn, A. G., Ichimoto, K., Fischer, C. E., Keller, C. U., & Lites, B. W. 2010, A&A, 519, A18
Trujillo Bueno, J., & Shchukina, N. 2007, ApJ, 664, L135
van Noort, M. 2012, A&A, 548, A5
van Noort, M., Rouppe van der Voort, L., & Löfdahl, M. G. 2005, Solar Phys., 228, 191
von der Luehe, O. 1993, A&A, 268, 374
Wöger, F., von der Lühe, O., & Reardon, K. 2008, A&A, 488, 375

A. Gandorfer (left) and A. Feller.